Applied Catalysis B: Environmental 308 (2022) 121212

Contents lists available at ScienceDirect

Applied Catalysis B: Environmental

journal homepage: www.elsevier.com/locate/apcatb

Enhanced catalytic elimination of typical VOCs over $ZnCoO_x$ catalyst derived from in situ pyrolysis of ZnCo bimetallic zeolitic imidazolate frameworks

Yunlong Guo [a,b], Meicheng Wen [a,b], Shengnan Song [a,b], Qiuxia Liu [a,b], Guiying Li [a,b], Taicheng An [a,b,*]

[a] Guangdong Key Laboratory of Environmental Catalysis and Health Risk Control, Guangdong Engineering Technology Research Center for Photocatalytic Technology Integration and Equipment, Institute of Environmental Health and Pollution Control, Guangdong University of Technology, Guangzhou 510006, China
[b] Guangdong-Hong Kong-Macao Joint Laboratory for Contaminants Exposure and Health, Guangzhou Key Laboratory of Environmental Catalysis and Pollution Control, School of Environmental Science and Engineering, Guangdong University of Technology, Guangzhou 510006, China

ARTICLE INFO

Keywords:
ZIFs-derived metal oxide
Zn-doped catalyst
Catalytic VOC elimination
Acid sites
VOCs with different chemical structures

ABSTRACT

In this work, $ZnCoO_x$ catalysts were prepared using in situ pyrolysis of ZnCo bimetallic zeolitic imidazolate frameworks (ZIFs), which were rationally designed on the basis of a metal ion doping strategy. The derived $Zn_{0.05}CoO_x$ with proper doping of Zn (Zn/Co molar ratio of 0.05) exhibited superior catalytic activity and durability towards catalytic elimination of different volatile organic compounds (VOCs) including benzene, toluene and cyclohexane under simulated real-exhaust conditions. Both Brønsted and Lewis acid sites were beneficial for cyclohexane degradation, whereas only Lewis acid sites were responsible for eliminations of benzene and toluene. In addition, the effect of chemical structures of VOCs on their catalytic elimination over $Zn_{0.05}CoO_x$ was explored. Compared to benzene and toluene, cyclohexane molecule was more easily eliminated, attributed to strong adsorption onto catalyst and special chemical structure of cyclohexane. The obtained results can provide new strategy for rational design of highly efficient catalytic materials for eliminating VOCs.

1. Introduction

Volatile organic compounds (VOCs) are ubiquitous in the ecosystem and mainly emitted from outdoor (industrial processes and transportation) and indoor sources (household products, construction materials, and cooking) [1–3]. Many of these VOCs, particularly the aromatics and alkanes, not only threaten human health and eco-environment, but are also regarded as the precursors of secondary pollutants, such as ozone and organic/inorganic secondary aerosols [4–6]. Therefore, the efficient purification of VOCs has attracted a lot of attention in recent years. The catalytic oxidation of VOCs is a promising approach, and includes technologies such as (thermo)catalysis, photocatalysis, and photothermocatalysis [2]. Although photocatalytic oxidation has the advantage of low energy consumption (by employing solar energy), it suffers easy deactivation and low catalytic efficiency [2,7]. Photothermocatalysis is essentially a light-driven (thermo)catalytic oxidation, which is also restricted by the shortcomings of photocatalysis [8]. Moreover, (thermo)catalytic oxidation of VOCs has the advantages of high elimination efficiency, few byproducts and outstanding catalytic stability, making it as an alternative removal technology for VOCs. However, the rational design of highly efficient catalytic materials is urgently required for removing VOCs [5,9]. Catalysts supported by noble metals are abundantly studied and applied for deep catalytic elimination of VOCs at lower temperatures. However, high cost of precious metal restricts their large-scale applications [4,10]. Recently, transition metal oxides were deemed as a promising alternative, however, the catalytic activity and stability of these catalysts remain a major challenge for effective elimination of VOCs.

Metal-organic frameworks (MOFs) have the advantages of high specific surface area, high porous structure and regular morphology, and are regarded as ideal precursors for the preparation of metal oxides. Moreover, the derived samples can effectively inherit the

* Corresponding author at: Guangdong Key Laboratory of Environmental Catalysis and Health Risk Control, Guangdong Engineering Technology Research Center for Photocatalytic Technology Integration and Equipment, Institute of Environmental Health and Pollution control, Guangdong University of Technology, Guangzhou 510006, China.
E-mail address: antc99@gdut.edu.cn (T. An).

https://doi.org/10.1016/j.apcatb.2022.121212
Received 20 December 2021; Received in revised form 6 February 2022; Accepted 11 February 2022
Available online 15 February 2022

physicochemical properties of the original MOFs through appropriate pyrolysis conditions [1,11,12]. Furthermore, the transformation of MOFs into metal oxides can realize the heteroatom doping at molecular level, which is vital to the derived catalyst for catalytic degradation of VOCs [13,14]. For instance, compared to CeO_2 and CuO that are derived from monometallic MOFs, mixed $CeCuO_x$ catalyst, which was derived from bimetallic MOFs, demonstrated enhanced catalytic activity for the oxidation of toluene [13]. Similar results were observed for the combustion of toluene over $CoCeO_x$, Co_3O_4/CeO_2 and CeO_2 catalysts [14]. Among different kinds of MOFs, zeolitic imidazolate frameworks (ZIFs) have been identified as ideal precursors for preparing catalysts in recent years. Additionally, the ZIFs-derived catalysts have demonstrated outstanding performance in various fields, such as VOC oxidation, CO_2 hydrogenation, and electrocatalysis [15–17]. For instance, this approach was used to prepare CuO/Co_3O_4 catalyst of the catalytic oxidation of toluene, which was derived from Cu ions and partly substituted framework of ZIF-67 [15].

It is commonly acknowledged that the surface acidity of a catalyst plays a crucial role in the adsorption and catalytic oxidation of VOCs [18,19]. Catalysts with abundant acid sites not only demonstrate high adsorption capacity for VOCs, but also exhibit strong capability for activating the C—H bonds during reaction with VOCs. With regards to the types of acid sites on the catalyst surface, Brønsted acid sites (proton donor) and Lewis acid sites (electron pair acceptor) are derived from hydroxyl groups and coordinatively unsaturated cation sites of the catalysts, respectively [20]. Although Brønsted and Lewis acid sites usually coexist on the sample, the two acid sites play different roles during the catalytic degradation of specific VOCs due to the properties of acid sites and the nature of VOCs. For example, Lv et al. [21] found that the increase in moderately strong Lewis acid sites on the surface of catalyst was beneficial to the activity and stability of CH_3Br oxidation. The rational design of various catalysts with a certain number of Brønsted and Lewis acid sites for catalytic degradation of VOCs is particularly important. Among various synthesis methods for catalysts, metal ion doping can be regarded as a novel and effective strategy for improving the acid sites of the samples. For instance, the addition of ZrO_2 to TiO_2 could increase the Lewis acidity of the supported catalyst, thus enhancing the thermal stability of the catalyst for oxidizing chlorobenzene [22]. The doping of Nb could also improve the number of Lewis acid sites of Ru/Nb/a-TiO_2 catalysts, which was beneficial for the oxidation of CH_3Br [21].

As for the air pollutants, over 300 chemicals are recognized as VOCs by the Environmental Protection Agency of USA, which are the major contributors to air pollution [23]. More importantly, the catalytic decomposition of VOCs is closely related to their chemical structures and corresponding properties [4,10,24]. Nevertheless, the majority of recent studies mainly focused on the preparation of catalysts and the structure-activity relationship [2,5,25]. Only a handful of studies have focused on the mechanism of the catalytic reaction of VOCs with different chemical structures. Furthermore, alkanes are the simplest organic pollutants, which contribute to a large proportion of the emitted VOCs in recent years. However, very few reports have paid attention to the catalytic degradation of alkane-based VOCs using metal oxides as catalysts [5].

Herein, the catalytic performance of ZnCo-ZIFs-derived catalysts for eliminating typical VOCs was demonstrated on the basis of the doping of a metal ion. In the strategy, the catalytically inactive Zn could be introduced into catalysts through in situ pyrolysis of bimetallic ZIFs. The original ZIFs and ZIFs-derived catalysts were characterized using a series of techniques to explore their compositions, morphologies, structures, adsorption, and acid sites. More importantly, three representative VOCs were selected to investigate the performance of the catalytic elimination of ZIFs-derived catalyst under simulated real-exhaust conditions. Moreover, the influence of the chemical structures of VOCs on their catalytic oxidation efficiencies was also systematically investigated. Furthermore, catalytic mechanism and kinetics of different VOCs were demonstrated. Most importantly, compared to traditional synthesis methods of metal oxides, the use of ZnCo-ZIFs as precursors of derived $ZnCoO_x$ catalysts not only realized proper molecular level doping of Zn, but also inherited the physicochemical properties of the original ZnCo-ZIFs. Overall, this work elucidates that the appropriate doping of Zn is favorable for catalytic activity of ZIFs-derived catalyst towards the oxidation of various VOCs, whereas the chemical structures of VOCs have a vital effect on their catalytic eliminations over the prepared catalyst.

2. Experimental

2.1. Sample preparation and characterization

ZnCo-ZIFs were synthesized according to a typical process with some modifications [26]. Briefly speaking, the mixture of $Zn(NO_3)_2.6\ H_2O$ and $Co(NO_3)_2.6\ H_2O$ with desired molar ratio of Zn^{2+}/Co^{2+} was dissolved in methanol (90 mL). Then, a mixture of 2-methylimidazole with 90 mL of methanol was quickly added to the above solution. The mixed solution was stirred violently under ambient temperature for 24 h. Finally, the product was centrifuged, washed with methanol for at least three times, and dried overnight under vacuum. Monometallic Co-ZIFs (known as ZIF-67) were prepared using the same method as described above except for the addition of $Zn(NO_3)_2.6\ H_2O$. The synthesized samples were named as ZnCo-ZIFs (n), where *n* represents the molar ratio of Zn/Co (n = 0, 0.025, 0.5, 0.1, 0.2 and 0.4). Furthermore, the ZIFs-derived metal oxide catalysts could be obtained using high-temperature pyrolysis of the corresponding ZnCo-ZIFs in air and stored at 350 °C for 3 h. These samples were denoted as Zn_nCoO_x (where *n* represents the molar ratio of Zn/Co). The calcination temperature of 350 °C was determined using the thermogravimetric analysis. Among various samples, the samples with the Zn/Co molar ratios of 0, 0.05 and 0.4 were chosen as the representative samples.

The properties of samples were characterized using various techniques including X-ray diffraction (XRD), thermogravimetric analysis (TGA), scanning electron microscopy (SEM), transmission electron microscopy (TEM), high-angle annular dark field-scanning transmission electron microscopy (HAADF-STEM), selected area electron diffraction (SAED), nitrogen adsorption–desorption, X-ray photoelectron spectroscope (XPS), inductively coupled plasma mass spectrometry (ICP-MS), Raman spectroscopy, hydrogen temperature-programmed reduction (H_2-TPR), VOC temperature-programmed desorption (VOC-TPD), and pyridine adsorbed IR spectroscopy (Py-IR). The detailed information about the instruments and their operating conditions are described in the Supplementary material.

2.2. Evaluation of the catalytic activity

Catalytic activity of the catalyst was evaluated in a fixed-bed reactor (internal diameter = 6 mm) under ambient pressure with online gas chromatography (GC) detection. The sample (50 mg) with the particle size of 40–60 mesh was packed in the reactor, and the gas mixture containing 1000 ppm VOCs + Air was introduced into the reaction system at a gas hourly space velocity (GHSV) of ca. 60,000 mL g^{-1} h^{-1}. Benzene, toluene and cyclohexane were chosen as the typical VOCs. The concentrations of VOCs were monitored using GC-9800 (Kechuang China), which was equipped with flame ionization detector. It is worth noticing that the catalytic performance of catalyst was analyzed under the condition that the feed gas stream always contained high content of water vapors. Approximately 5.0 vol% of water vapor was introduced into the reaction system by passing the reactant gas through a water saturator at 33 °C. The balance of carbon was above 98.0% during the degradation of VOCs. As for the evaluation of the catalytic performance of the catalyst, the mineralization of VOCs was calculated according to Eq. (1).

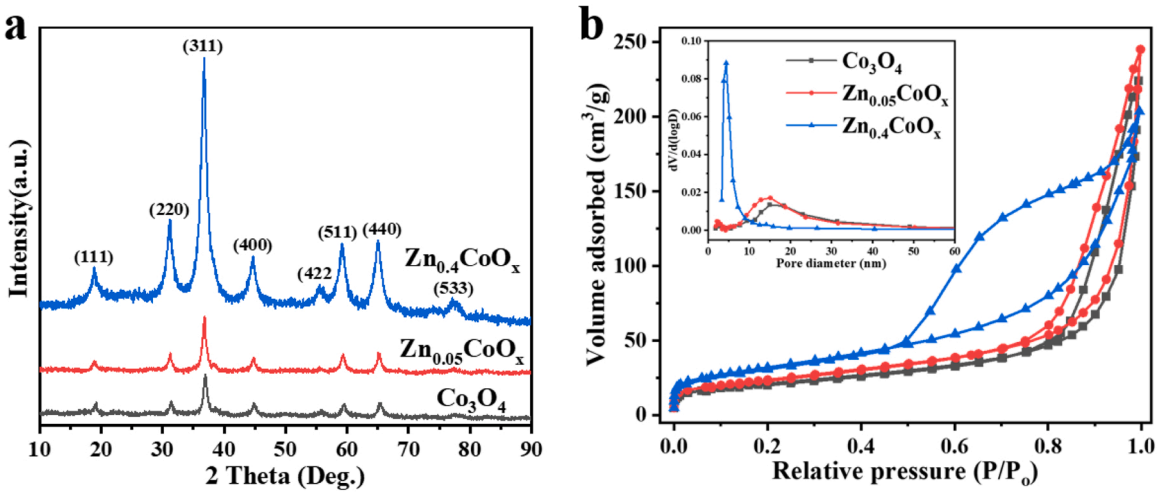

Fig. 1. (a) XRD patterns and (b) nitrogen adsorption-desorption isotherms and the corresponding pore size distributions (inset) of Co_3O_4, $Zn_{0.05}CoO_x$ and $Zn_{0.4}CoO_x$.

$$\text{VOC mineralization} = \frac{[CO_2]_{out}}{n \times [VOC]_{in}} \times 100\% \quad (1)$$

where $[VOC]_{in}$ is the inlet molar quantity of vaporous VOCs, $[CO_2]_{out}$ is the outlet molar quantity of CO_2, and n represents the number of carbon atoms in the corresponding molecular formula of VOCs including benzene, toluene and cyclohexane.

3. Results and discussion

3.1. Structural characterization of prepared sample

Thermogravimetric analysis (TGA) in air flow shows that all the three ZIFs (ZIF-67, ZnCo-ZIFs (0.05) and ZnCo-ZIFs (0.4)) started to decompose at around 266 °C (Fig. S1a). The samples were heated with continuously increasing the temperature during the whole TGA tests. In this regard, 350 °C was selected for the substantial transformation of various ZIFs into metal oxide catalysts. The color of ZnCo-ZIFs (0.05) was purple whereas that of $Zn_{0.05}CoO_x$ was black, which manifested the successful pyrolysis of bimetallic ZIFs into metal oxide catalyst (Fig. S2). In addition, TGA characterizations of the three derived metal oxide catalysts were also conducted (Fig. S1b), indicating good thermal stability of this kind of catalysts. Based upon the XRD patterns, the crystalline structures confirm that the three derived catalysts (Co_3O_4, $Zn_{0.05}CoO_x$ and $Zn_{0.4}CoO_x$) possessed similar diffraction peaks (Fig. 1a). They were ascribed to the reflections of (111), (220), (311), (400), (422), (511), (440) and (533) lattice planes of Co_3O_4, respectively (JCPDS PDF#43-1003) [27,28]. No ZnO peaks were detected from the XRD patterns of $Zn_{0.05}CoO_x$ and $Zn_{0.4}CoO_x$, which can be ascribed to the low doping and good dispersion of Zn on the catalyst. In addition, XRD patterns of the derived metal oxide catalysts with other Zn/Co ratios were also obtained (Fig. S3), which were consistent with the results presented in Fig. 1a.

Furthermore, the changes in the lattice structures of catalysts were explored using Raman spectrum. All the derived catalysts exhibited five typical absorption peaks, corresponding to different modes of Co_3O_4 (Fig. S1c). Compared to the undoped Co_3O_4, the band shapes of Zn-doped catalysts broadened and weakened, which were related to the lattice distortion of the spinel structure [29]. Besides, the band positions of $ZnCoO_x$ exhibited slight red-shifting, indicating that the samples had undergone structural changes such as lattice defects [30]. Therefore, the Raman spectra results imply that Zn species were successfully incorporated into the lattice of CoO_x over $ZnCoO_x$ catalysts. Besides, the XRD patterns of all ZnCo-ZIFs showed similar characteristic peaks, which matched well with the simulated ZIF-67 (Fig. S1d) due to similar unit cells and crystal lattices [26]. The ICP-MS analyses of $Zn_{0.05}CoO_x$ and $Zn_{0.4}CoO_x$ demonstrate that the actual values of Zn/Co molar ratios were 0.049 and 0.379, which were close to the theoretical values of 0.05 and 0.4, respectively.

Nitrogen (N_2) adsorption-desorption isotherms and pore size distributions of the samples are shown in Fig. 1b. All the ZIFs-derived catalysts exhibited a Type IV N_2 physisorption isotherm, with hysteresis loops being found at relative pressures (P/P_0) of 0.50–0.99, which was a proof of the presence of mesoporous structure [31,32]. Moreover, both Co_3O_4 and $Zn_{0.05}CoO_x$ presented a H1 hysteresis loop, indicating that the derived mesoporous samples had relatively narrow pore size distributions and spherical particle aggregates with relatively uniform sizes [31]. However, $Zn_{0.4}CoO_x$ showed a H2 hysteresis loop, implying the existence of ink-bottle pores with wide bodies and narrow necks [31]. Compared to original ZIFs with micropores (Fig. S4 and Table S1), the transformation from micropore to mesopore could be efficiently achieved through thermal calcination process, whereas the specific surface area of derived catalysts is tempestuously decreased, indicating the collapse of ZIFs framework structure [27]. Based on the pore size distribution profile (the inset of Fig. 1b), the pore sizes of maximum adsorption peaks decreased in the descending order of: Co_3O_4 > $Zn_{0.05}CoO_x$ > $Zn_{0.4}Co_3O_4$, which implied that more Zn doping could promote the aggregation of crystalline particles and reduce the pore size of derived catalysts. The detailed textural properties of the derived catalysts are presented in Table 1. With the increase of Zn doping, the

Table 1
Textural properties and surface species of the catalysts.

Sample	BET specific surface area ($m^2\ g^{-1}$)	Pore volume[a] ($cm^3\ g^{-1}$)	Pore diameter[b] (nm)	$Co^{3+}/(Co^{3+}+Co^{2+})$[c] (%)	$O_{ads}/(O_{ads}+O_{latt})$[c] (%)
Co_3O_4	74	0.35	20.3	49.0	47.7
$Zn_{0.05}CoO_x$	85	0.38	17.9	58.9	51.1
$Zn_{0.4}CoO_x$	114	0.31	6.5	55.7	47.9

[a] Calculated from the volume adsorbed at $P/P_0 = 0.99$.
[b] Calculated from the desorption branch of nitrogen isotherm by using the BJH model.
[c] Calculated from the XPS data.

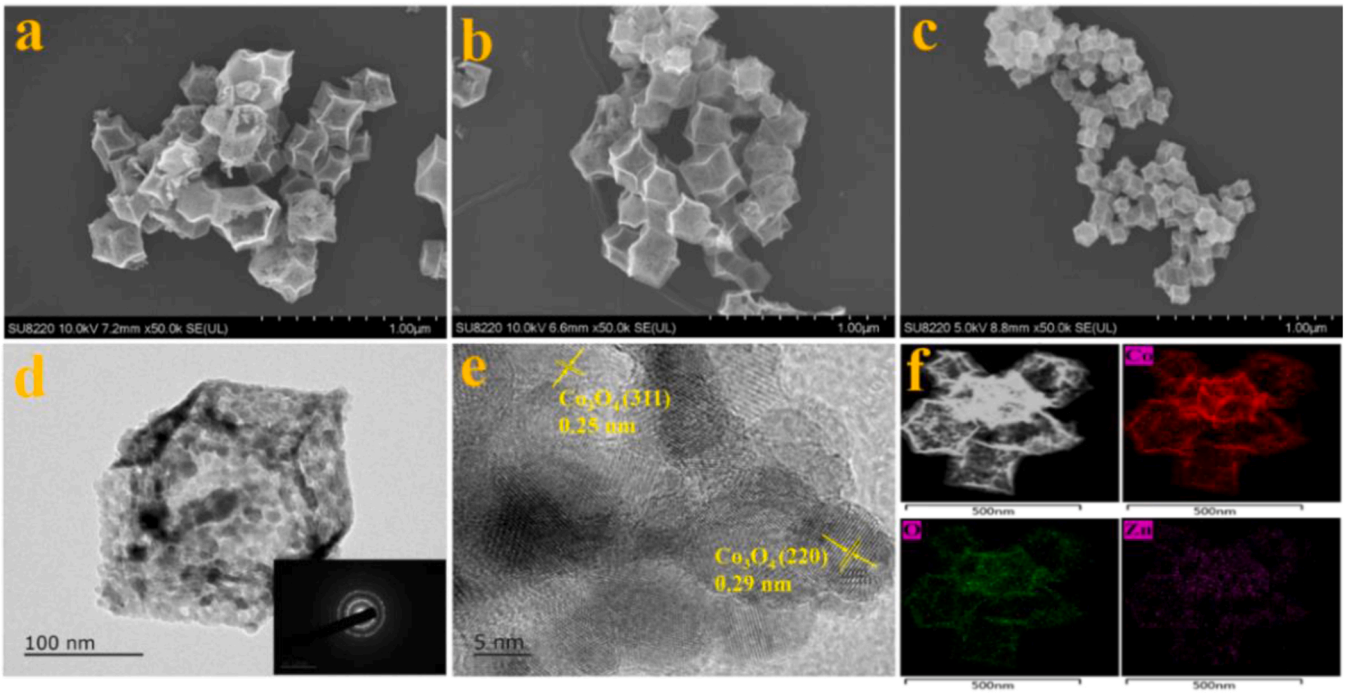

Fig. 2. SEM images of (a) Co_3O_4, (b) $Zn_{0.05}CoO_x$ and (c) $Zn_{0.4}CoO_x$; For $Zn_{0.05}CoO_x$: (d) TEM and its SAED pattern in the inset, (e) HRTEM and (f) STEM-EDS elemental mapping.

specific surface area of samples increased. However, the average pore diameter became smaller. This can be ascribed to the decreased crystallinity of the derived catalyst, which was induced by Zn doping, and resulted in the alteration of specific surface area and pore size [27]. Compared with other MOFs-templated or Co-based catalysts [27,33], the ZIFs-derived catalysts displayed high specific surface areas of 74–114 $m^2\ g^{-1}$, indicating the advantage of using ZnCo-ZIFs as the precursors for catalyst synthesis.

According to the SEM images of ZIFs with different Zn/Co molar ratios (Fig. S5), the particle size of dodecahedron over ZIFs became smaller with the increase in Zn/Co molar ratio. This means that the molar ratio of Zn/Co is a key factor for the particle size of ZIFs crystals. As for the representative ZnCo-ZIFs (0.05), both the elements of Zn and Co were evenly dispersed on the sample, whereas Co content was much higher than that of Zn (Fig. S6). This result is consistent with the molar ratio of Zn/Co, which was measured using ICP-MS. In addition, the transformation of ZIFs into metal oxide catalysts did not lead to substantial change in morphology, while the corresponding particle sizes of polyhedron became smaller than that of original ZIFs (Fig. 2a–c), which are presumably due to the shrinkage of the whole ZIFs caused by high-temperature calcination. Accordingly, when the calcination temperature was 350 °C, the ZIFs-derived catalysts successfully retained the polyhedron structure of original ZIFs.

The $Zn_{0.05}CoO_x$ was further characterized using TEM. The results showed that the surface of the catalyst consisted of numerous crystal nanoparticles, on which the mesopores could be clearly observed (Fig. 2d). The bright electron diffraction rings in the SAED pattern indicated the formation of polycrystalline structures of the catalyst (Fig. 2d, inset). In addition, the high magnification image shown in Fig. 2e demonstrated the exposure of (311) plane and (220) plane of Co_3O_4 [27]. STEM-EDS elemental mapping (Fig. 2f) indicates that the doped Zn was uniformly dispersed throughout the catalyst, demonstrating the reasonable doping of Zn into the catalyst.

3.2. Catalytic elimination of different VOCs

The catalytic performances of Co_3O_4, $Zn_{0.05}CoO_x$ and $Zn_{0.4}CoO_x$ for the degradation of three typical VOCs were evaluated. As shown in Fig. 3a–c, $Zn_{0.05}CoO_x$ exhibited the best mineralization activity towards the elimination of different VOCs (including benzene, toluene and cyclohexane) in the presence of 5.0 vol% water vapors at various temperatures, followed by Co_3O_4 and $Zn_{0.4}CoO_x$. As a comparison, the catalytic degradations of the three different VOCs over $Zn_{0.05}CoO_x$ catalyst was also carried out under the feed gas containing 5.0 vol% water vapors (Fig. 3d), and the temperatures required for 90% mineralization (T_{90}) of benzene, toluene, and cyclohexane were determined to be 237, 252 and 234 °C, respectively. The detailed description of the catalytic evaluation data is presented in Table S2. Besides, the specific reaction rates of the three VOCs over different catalysts were also calculated. On the basis of BET specific surface area of the catalysts, both the Co_3O_4 and $Zn_{0.05}CoO_x$ exhibited higher specific reaction rates than that of $Zn_{0.4}CoO_x$ (Fig. S7). The aliphatic hydrocarbons exhibit lower mineralization temperatures than those of aromatics, which may be ascribed to simultaneous abstraction of hydrogen from phenyl and methyl groups on 4–5 adjacent oxygen sites towards the oxidation of aromatics [34]. Furthermore, the mineralization of various VOCs using different catalysts in the absence of water vapors was also evaluated (Fig. S8 and Table S3). The results show that the water vapors had little influence on the catalytic performances of ZIFs-derived catalysts for the elimination of benzene, toluene and cyclohexane during the whole catalytic elimination process, which is in favor of real exhaust elimination in practical atmospheric environment. Moreover, benzene was selected as a model pollutant to investigate the influence of Zn/Co molar ratio of the ZIFs-derived catalyst on the catalytic performance of the process (Fig. S9). The results showed that Zn/Co molar ratio of 0.05 was optimum for various ZnCo-ZIFs-derived catalyst. In addition, the optimal $Zn_{0.05}CoO_x$ catalyst also exhibited superior catalytic performance than previously reported catalysts for the catalytic elimination of benzene, toluene and cyclohexane (Table S4).

The catalytic endurance of a catalyst is a very crucial evaluation index for the degradation of VOCs in practical applications. Therefore, the catalytic durability of the optimal $Zn_{0.05}CoO_x$ for catalytic elimination of benzene, toluene and cyclohexane was conducted under the feed gas containing 5.0 vol% water vapors. As shown by Fig. 4, the catalytic

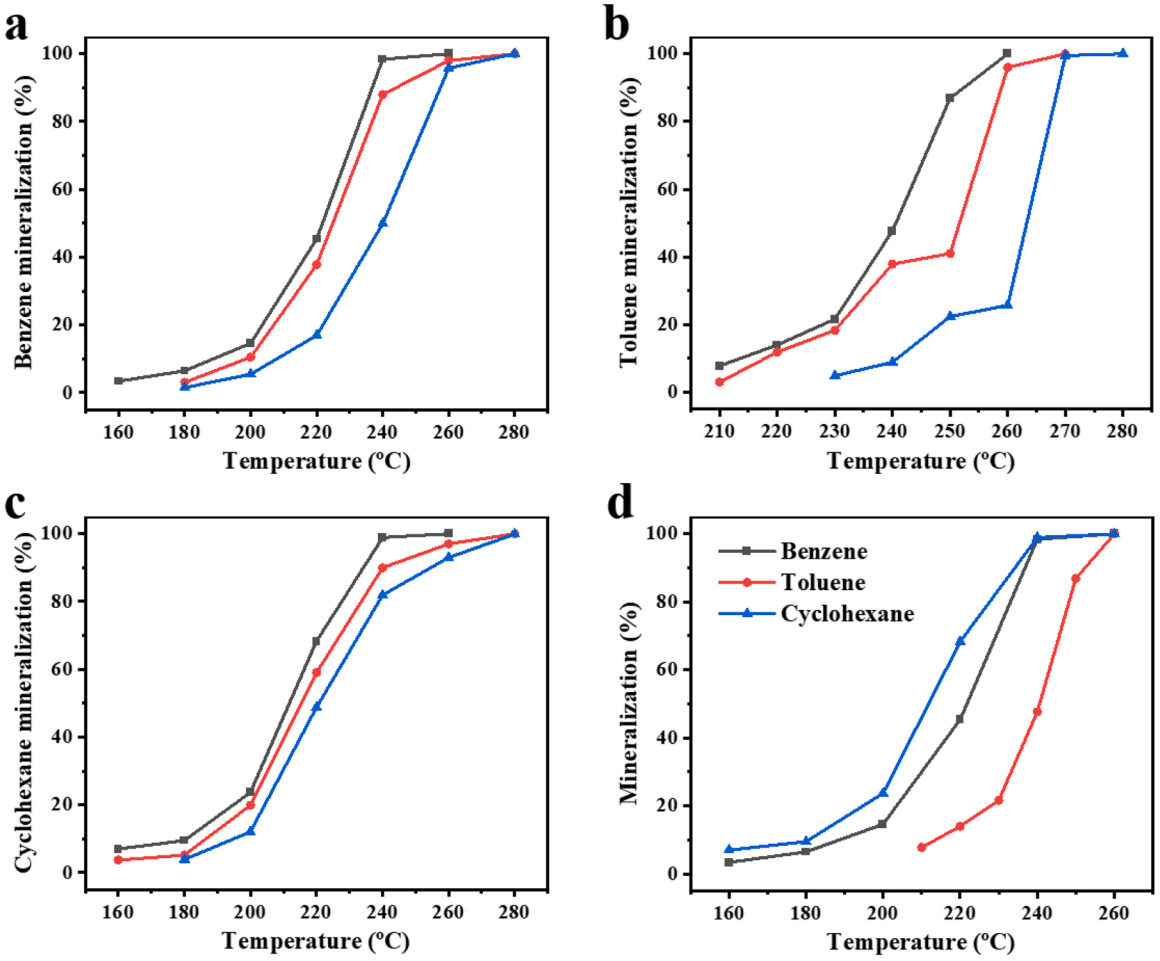

Fig. 3. (a) Benzene, (b) toluene and (c) cyclohexane mineralization as a function of reaction temperature catalyzed by Co_3O_4 (red), $Zn_{0.05}CoO_x$ (black) and $Zn_{0.4}CoO_x$ (blue); (d) The profile for catalytic mineralization of benzene, toluene and cyclohexane over $Zn_{0.05}CoO_x$ catalyst. Note: 5.0 vol% of water vapor, VOC = 1000 ppm and GHSV = 60,000 mL g^{-1} h^{-1}.

mineralization of benzene, toluene and cyclohexane within the range of 60–80% remained unchanged during 30 h for the reaction temperatures of 225, 245 and 220 °C, respectively, demonstrating that $Zn_{0.05}CoO_x$ is catalytically and thermally stable for the catalytic elimination of various VOCs under the conditions of high water vapor content. In addition, based on the XRD and SEM characterizations (Figs. S10 and S11), the crystal structure and morphology of $Zn_{0.05}CoO_x$ catalyst after 30 h of continuous VOC elimination in the presence of 5.0 vol% water vapor were the same as the original catalyst, implying the excellent stability and durability of ZIFs-derived catalyst for long-time on-stream reaction in practical applications.

3.3. Reducibility characterization and surface acidity assessment

XPS analysis can efficiently reflect the surface elemental composition, metal oxidation states and oxygen species of the samples. Herein, XPS spectra were analyzed for the ZIFs-derived catalysts. The full XPS spectra are presented in Fig. S12, proving that Co and O existed on the surface of Co_3O_4. Moreover, the elements of Co, O and Zn existed on the surfaces of $Zn_{0.05}CoO_x$ and $Zn_{0.4}CoO_x$. As shown in Fig. 5a, the Co 2p demonstrated two peaks at 779.6 and 781.3 eV, which corresponded to Co^{3+} and Co^{2+}, respectively [27]. A peak fit software was used to calculate the molar ratios of the species. As shown in Table 1, the Zn-doped catalysts had higher values of $Co^{3+}/(Co^{3+}+Co^{2+})$, indicating that the doping of Zn could change the valence of cobalt species. This result further supported high VOC degradation capability of the catalysts, because Co^{3+} species is regarded as the active sites of catalysts towards the degradation of VOCs [33]. With respect to O 1s species, three peaks could be observed at 529.5, 531.7 and 533.2 eV (Fig. 5b), which were ascribed to lattice oxygen species (O_{latt}), adsorbed oxygen species (O_{ads}) and hydroxyl species/adsorbed water, respectively [35]. The highest $O_{ads}/(O_{ads}+O_{latt})$ was observed for $Zn_{0.05}CoO_x$ (Table 1). It is generally accepted that O_{ads} species usually have higher mobility than O_{latt} and participate as active sites of catalysts for the oxidation of VOCs [36]. In addition, the Zn 2p spectra over $Zn_{0.05}CoO_x$ and $Zn_{0.4}CoO_x$ were also analyzed (Fig. S13). The binding energies centered at 1021.0 and 1044.2 eV belonged to Zn $2p_{3/2}$ and Zn $2p_{1/2}$, respectively, which were assigned to Zn^{2+} species [37]. This result elucidates that Zn element has been successfully doped into the catalyst and appears in oxidized state on the catalyst.

Since the oxidation of VOCs is correlated with the redox properties of the catalyst, the H_2-TPR measurements were conducted to explore the influence of Zn/Co molar ratio on the reducibility of ZIFs-derived catalysts. As shown in Fig. 6, three reduction peaks were observed for Co_3O_4, $Zn_{0.05}CoO_x$ and $Zn_{0.4}CoO_x$ catalysts. The first reduction peak at around 200 °C was assigned to the consumption of reactive oxygen species, which were adsorbed onto the surface oxygen vacancies of the samples [38]. The second and third reduction peaks appeared within the range of 297–421 °C, and attributed to the stepwise reduction of $Co^{3+}\rightarrow Co^{2+}\rightarrow Co^0$. It is observed that, with the increase of Zn doping in Co_3O_4, $Zn_{0.05}CoO_x$ and $Zn_{0.4}CoO_x$, the reduction temperatures of the corresponding peaks shifted to higher values. According to the

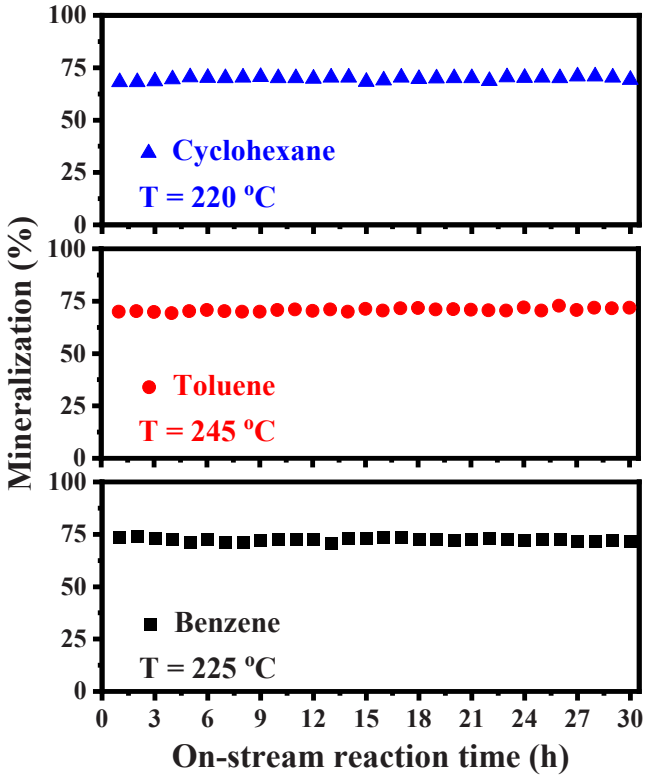

Fig. 4. Durability tests of benzene, toluene and cyclohexane mineralization catalyzed by $Zn_{0.05}CoO_x$ catalyst at 225, 245 and 220 °C, respectively. Note: 5.0 vol% of water vapor, VOC = 1000 ppm and GHSV = 60,000 mL g^{-1} h^{-1}.

oxidation-reduction mechanism [6,39], such shifts demonstrate the strong interaction between Co and doped Zn. The H_2-TPR results demonstrate that such interactions decrease the reducibility of the doped catalysts, which are unfavorable for the catalytic activity of the catalysts. Therefore, the molar ratio of Zn/Co is an important factor for the determination of redox capabilities of ZIFs-derived catalysts. In general, low temperature reducibility of catalysts is beneficial for the catalytic performance towards the oxidation of VOCs.

It is generally accepted that acid sites are regarded as the active sites on the surface of metal oxide catalysts [5]. Therefore, Py-IR characterizations were performed for the three catalysts to distinguish and quantify the acid sites on the surface of the catalysts. The Py-IR spectra of pyridine adsorption on the catalyst showed five characteristic peaks (Fig. 7). The absorption bands at 1447 and 1609 cm^{-1} were assigned to pyridine adsorption on Lewis acid sites, whereas the bands at 1540 and 1637 cm^{-1} were ascribed to pyridine adsorbed onto the Brønsted acid sites [40]. It is worth noticing that the band at about 1489 cm^{-1} was ascribed to pyridine adsorbed onto both Brønsted and Lewis acid sites [40]. Generally speaking, the absorption band at 1450 cm^{-1} is used to quantify the Lewis acid sites, whereas the number of Brønsted acid sites can be calculated from the peak areas centered at 1540 cm^{-1} [41]. The results presented in Table 2 show that $Zn_{0.05}CoO_x$ catalyst processed the highest concentration of acid sites due to the contribution of high-concentration Lewis acid sites, followed by those of Co_3O_4 and $Zn_{0.4}CoO_x$. Moreover, Zn doping had an important influence on the surface acidity of the catalyst. In this regard, the Brønsted acid sites would be considerably replaced with Lewis acid sites after proper Zn doping (Zn/Co molar ratio of 0.05) due to highly dispersed Zn species of the prepared catalyst [42]. Nevertheless, it is speculated that too much Zn doping (Zn/Co molar ratio of 0.4) would cause the agglomeration of Zn species on the catalyst, which is not conducive to the generation of Lewis acid sites. Therefore, the results presented in Table 2 show that, an appropriate doping of Zn can obviously increase the Lewis acid sites of the catalysts, and eventually, increase the total acid sites. Similar results

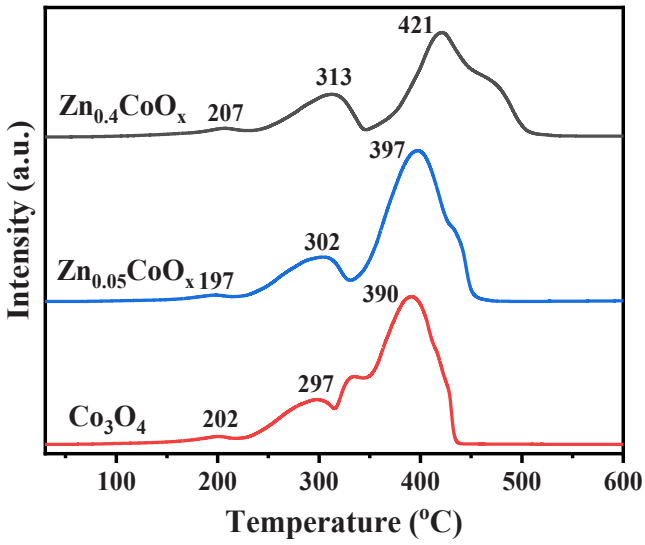

Fig. 6. H_2-TPR profiles of Co_3O_4, $Zn_{0.05}CoO_x$ and $Zn_{0.4}CoO_x$.

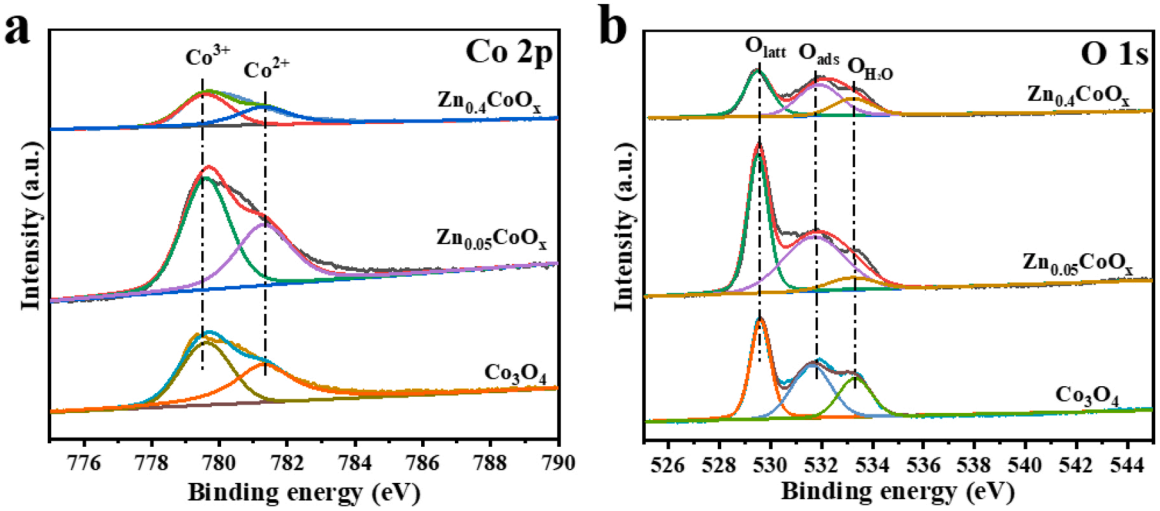

Fig. 5. XPS spectra of (a) Co 2p and (b) O 1s for Co_3O_4, $Zn_{0.05}CoO_x$ and $Zn_{0.4}CoO_x$ catalysts.

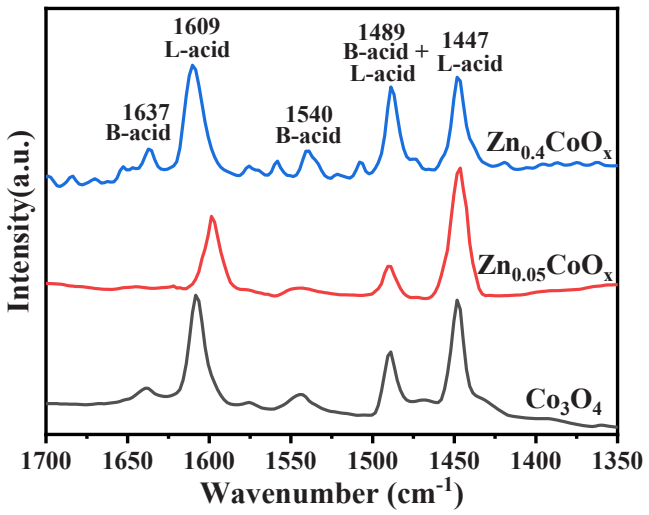

Fig. 7. Py-IR spectra of Co_3O_4, $Zn_{0.05}CoO_x$ and $Zn_{0.4}CoO_x$ at 150 °C.

Table 2
Concentration of acid sites of three different catalysts at 150 °C.

Sample	$C_{Brønsted}$ (μmol g^{-1})	C_{Lewis} (μmol g^{-1})	C_{total} (μmol g^{-1})	C_{Lewis}/ $C_{Brønsted}$
Co_3O_4	17.4	71.2	88.5	4.1
$Zn_{0.05}CoO_x$	16.3	97.7	114.0	6.0
$Zn_{0.4}CoO_x$	22.2	62.9	85.1	2.8

could be also observed when the samples were vacuumed at 300 °C (Fig. S14 and Table S5).

The abundant Brønsted and Lewis acid sites on the surface of catalyst can obviously enhance the low-temperature catalytic activity of the catalyst towards the elimination of various VOCs [21,43]. Combining the results with those shown in Fig. 3, it can be inferred that $Zn_{0.05}CoO_x$ catalyst with the highest concentration of Brønsted and Lewis acid sites exhibited superior catalytic performance towards the catalytic oxidation of benzene, toluene and cyclohexane as compared to Co_3O_4 and $Zn_{0.4}CoO_x$. It is worth noticing that cyclohexane molecule can be more easily eliminated over the same catalysts, followed by benzene and toluene. This may be due to the acid sites of the catalysts as well as the types of VOCs with different chemical structures. The aromatic molecules with the characteristic of benzene ring can be deemed as Lewis basic hydrocarbons, of which aromatics are adsorbed on the derived metal oxide catalysts by the acid-base interaction between the Lewis base aromatics and the Lewis acid sites of the catalyst [18,19]. On the contrary, it is speculated that cyclohexane molecules with C—C bonds demonstrated two reaction pathways with the acid sites on the surface of the derived catalyst. The cyclohexane molecules could be converted to non-classical five-coordinated carbonium ions through protonation effect of the Brønsted acid sites, whereas classical carbonium ions would be generated due to the loss of H^- from cyclohexane molecules through the capture of Lewis acid sites [44]. Then, the two types of carbonium ions would be converted to intermediate species as well as final products over the catalyst [41]. On the basis of this analysis, it is implied that both the Brønsted and Lewis acid sites are beneficial for the catalytic elimination of cyclohexane. Nevertheless, only the Lewis acid sites are responsible for the oxidation of benzene and toluene. Therefore, in comparison to the catalytic elimination of aromatics (benzene and toluene), the cyclohexane could be more effectively degraded under same conditions.

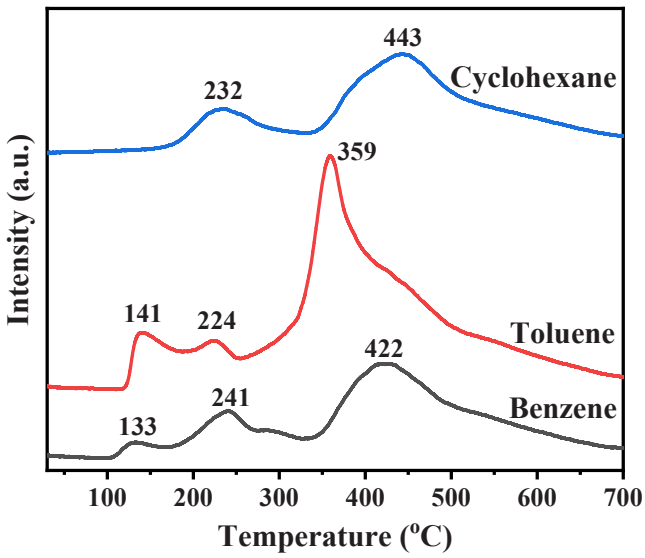

Fig. 8. VOC-TPD profiles of benzene, toluene and cyclohexane over $Zn_{0.05}CoO_x$ catalyst.

3.4. Comparison of catalytic mechanism and kinetics of VOC elimination

In order to explore the adsorption-desorption and oxidation capability of catalyst for benzene, toluene and cyclohexane, the VOC-TPD experiments were performed. As shown in Fig. 8, the peaks at the temperature of 130–250 °C can be ascribed to the desorption of weakly adsorbed VOCs. For these, the desorption temperature was almost identical for the three VOCs. However, for the desorption of strongly adsorbed VOCs (350–450 °C), the desorption temperatures of VOCs over $Zn_{0.05}CoO_x$ decreased in the descending order of: cyclohexane > benzene > toluene. Generally, a higher desorption temperature indicates a stronger adsorption, and thus, easier catalytic oxidation of VOCs [45]. Therefore, this result can elucidate that cyclohexane molecule is more inclined to be catalytically degraded due to stronger adsorption capability than those of benzene and toluene. With regards to the interaction between the catalyst and the VOCs, it is deduced that the adsorption of aromatics (benzene and toluene) over $Zn_{0.05}CoO_x$ catalyst can be assigned to cation-π interaction due to the characteristics of the benzene ring. However, the adsorption of cyclohexane may be ascribed to van der Waals interactions due to the characteristics of a typical aliphatic hydrocarbon [11,46]. Therefore, the chemical structures of VOCs play a crucial role in determining the interactions between the VOCs and the catalysts.

Typically, the reaction mechanism for the oxidation of VOCs can be explained by three kinetic models including Langmuir-Hinshelwood (L-H) model, Eley-Rideal (E-R) and Mars-van Krevelen (MvK) model [2]. The applicable catalytic reaction mechanism depends on both the properties of the catalyst and the nature of VOC molecules. According to the definitions of the three models, the adsorbed oxygen species are regarded as the main reactive species for both the L-H and E-R models, whereas lattice oxygen species can be deemed as the main reactive species for the MvK model [47]. Based upon the VOC-TPD spectra (Fig. 8), it can be inferred that all the three VOC molecules can be easily adsorbed on the surface of $Zn_{0.05}CoO_x$, which indicates that the degradation of VOCs possibly follows the L-H or MvK model. In addition, after removing the adsorbed oxygen species on the surface of catalyst with helium gas [47], the VOC-TPD spectra still maintained the desorption peaks of VOCs even at high temperature. Therefore, it is implied that the three VOC molecules were difficult to oxidize in the absence of adsorbed oxygen species on the catalyst, indicating that the lattice oxygen species could not react with the VOC molecules. Based on these results, the catalytic reaction mechanism for the oxidation of three VOC molecules

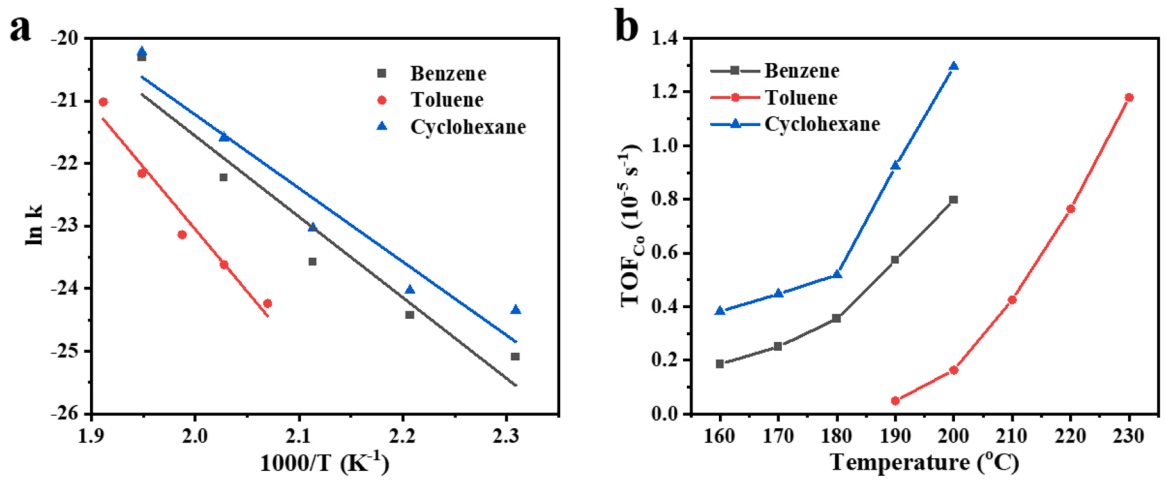

Fig. 9. (a) Arrhenius plot and (b) TOF_{Co} of catalytic elimination of benzene, toluene and cyclohexane over $Zn_{0.05}CoO_x$ catalyst in the presence of 5.0 vol% water vapor.

was found to follow the L-H model. The adsorbed VOC molecules reacted with the adsorbed oxygen species, as a result, the intermediates and final products were produced.

Presently, many studies have reported the catalytic elimination of VOCs [2,5]. Nevertheless, the calculations and comparison of catalytic elimination for different VOCs are rarely discussed. Therefore, in this paper, the kinetic studies were demonstrated to explain the influence of the chemical structure of VOCs on the catalytic degradation of the catalyst. It is speculated that the catalytic degradation of the three different VOCs may follow the first-order kinetic mechanism in the presence of excess oxygen, which is relevant to the concentrations of VOCs and oxygen [48]. The Arrhenius plots for the degradations of three VOCs over $Zn_{0.05}CoO_x$ under the impact of a feed gas stream containing 5.0 vol% of water vapors were drawn (Fig. 9a). The apparent activation energy (E_a) values for the degradation of VOCs were obtained from the slopes of the Arrhenius plots. The E_a value for cyclohexane was found to be 97.7 kJ mol^{-1}, which was lower than those of benzene (107.4 kJ mol^{-1}) and toluene (165.3 kJ mol^{-1}). It is well-known that lower E_a usually implies lower reaction energy barrier for the degradation of VOCs (such as C—H bond dissociation energy) and stronger conductibility for catalytic elimination of VOCs, which are ultimately beneficial for eliminating the VOCs [20,49]. In addition, the values of TOF_{Co} increased with the increase in temperature even when the gas stream contained 5.0 vol% water vapors (Fig. 9b). Cyclohexane showed the highest elimination efficiency, followed by benzene and toluene. Overall, the catalytic degradation of cyclohexane over $Zn_{0.05}CoO_x$ had the highest TOF_{Co} as well as the lowest E_a value in the presence of 5.0 vol % water vapors, which could be ascribed to the special chemical structure of cyclohexane and strong adsorption of cyclohexane onto the catalyst. Unlike cyclohexane that has only the C—H single bond, the degradation of aromatics needed to destroy the aromatic ring, which is the main reason for slower catalytic reaction [33,34]. The difference in the chemical structures of toluene and benzene is that toluene has an added methyl group. Moreover, the degradation of toluene molecule required simultaneous abstraction of H atoms from the phenyl and methyl groups [34,50]. Therefore, the catalytic degradation of toluene was more difficult than benzene, due to the steric hindrance of methyl groups.

4. Conclusions

The transformation of ZnCo bimetallic ZIFs into $ZnCoO_x$ was successfully conducted using Zn doping strategy via in situ pyrolysis. The synthesized $ZnCoO_x$ catalysts were applied for the catalytic elimination of three typical VOCs. The results show that, compared to the reference catalysts of Co_3O_4 and $Zn_{0.4}CoO_x$, proper doping of Zn can obviously enhance the catalytic performance of $Zn_{0.05}CoO_x$ for the catalytic elimination of benzene, toluene and cyclohexane in the presence of 5.0 vol% water vapors. In addition, $Zn_{0.05}CoO_x$ also exhibited excellent catalytic durability for at least 30 h of on-stream reaction under high content of water vapor. The excellent catalytic activity and durability of $Zn_{0.05}CoO_x$ catalyst can be attributed to high concentration of Co^{3+} and O_{ads} species, good low-temperature reducibility, abundant acid sites as well as strong interaction between Co and Zn. Besides, Brønsted and Lewis acid sites on the surface of the catalyst play an important role in the catalytic elimination of typical VOCs with different chemical structures. Both the Brønsted and Lewis acid sites are beneficial for the catalytic elimination of cyclohexane. However, only Lewis acid sites are responsible for the catalytic oxidation of benzene and toluene. Furthermore, the mineralization of cyclohexane catalyzed by $Zn_{0.05}CoO_x$ had the lowest T_{90} of 234 °C in the presence of 5.0 vol% water vapors, followed by those of benzene and toluene. Overall, this study demonstrates that typical VOCs can be effectively eliminated using MOFs-derived metal oxide catalysts under the simulated exhaust conditions, which will provide theoretical and experimental foundations for controlling the atmospheric pollution in real-world environment.

CRediT authorship contribution statement

Yunlong Guo: Investigation, Data curation, Formal analysis, Writing – original draft. **Meicheng Wen**: Methodology, Formal analysis, Writing – review & editing. **Shengnan Song:** Validation, Software. **Qiuxia Liu**: Data curation, Methodology. **Guiying Li:** Visualization, Supervision, Writing – review & editing. **Taicheng An**: Conceptualization, Supervision, Funding acquisition, Writing – review & editing.

Declaration of Competing Interest

The authors declare that they have no known competing financial interests or personal relationships that could have appeared to influence the work reported in this paper.

Acknowledgments

This work was supported by Guangdong Provincial Key R&D Program (2019B110206002), National Natural Science Foundation of China (42007192 and 42077332), Local Innovative and Research Teams Project of Guangdong Pearl River Talents Program (2017BT01Z032), and China Postdoctoral Science Foundation (2020M682618).

Appendix A. Supplementary material

Supplementary data associated with this article can be found in the online version at doi:10.1016/j.apcatb.2022.121212.

References

[1] Q. Wang, Y. Li, A. Serrano-Lotina, W. Han, R. Portela, R. Wang, M. Bañares, K. L. Yeung, Operando investigation of toluene oxidation over 1D Pt@CeO_2 derived from Pt custer-containing MOF, J. Am. Chem. Soc. 143 (2020) 196–205.

[2] Y. Guo, M. Wen, G. Li, T. An, Recent advances in VOC elimination by catalytic oxidation technology onto various nanoparticles catalysts: a critical review, Appl. Catal. B Environ. 281 (2021), 119447.

[3] H. Peng, T. Dong, S. Yang, H. Chen, Z. Yang, W. Liu, C. He, P. Wu, J. Tian, Y. Peng, X. Chu, D. Wu, T. An, Y. Wang, S. Dai, Intra-crystalline mesoporous zeolite encapsulation-derived thermally robust metal nanocatalyst in deep oxidation of light alkanes, Nat. Commun. 13 (2022) 1–10.

[4] C. Yang, G. Miao, Y. Pi, Q. Xia, J. Wu, Z. Li, J. Xiao, Abatement of various types of VOCs by adsorption/catalytic oxidation: a review, Chem. Eng. J. 370 (2019) 1128–1153.

[5] C. He, J. Cheng, X. Zhang, M. Douthwaite, Z. Hao, Recent advances in the catalytic oxidation of volatile organic compounds: a review based on pollutant sorts and sources, Chem. Rev. 119 (2019) 4471–4568.

[6] Y. Guo, Y. Gao, X. Li, G. Zhuang, K. Wang, Y. Zheng, D. Sun, J. Huang, Q. Li, Catalytic benzene oxidation by biogenic Pd nanoparticles over 3D-ordered mesoporous CeO_2, Chem. Eng. J. 362 (2019) 41–52.

[7] H. Liu, Y. Ma, J. Chen, M. Wen, G. Li, T. An, Highly efficient visible-light-driven photocatalytic degradation of VOCs by CO_2-assisted synthesized mesoporous carbon confined mixed-phase TiO_2 nanocomposites derived from MOFs, Appl. Catal. B Environ. 250 (2019) 337–346.

[8] Y. Li, S. Wu, J. Wu, Q. Hu, C. Zhou, Photothermocatalysis for efficient abatement of CO and VOCs, J. Mater. Chem. A 8 (2020) 8171–8194.

[9] Q. Wang, K.L. Yeung, M.A. Bañares, Ceria and its related materials for VOC catalytic combustion: a review, Catal. Today 356 (2020) 141–154.

[10] Z. Wang, P. Ma, K. Zheng, C. Wang, Y. Liu, H. Dai, C. Wang, H.-C. Hsi, J. Deng, Size effect, mutual inhibition and oxidation mechanism of the catalytic removal of a toluene and acetone mixture over TiO_2 nanosheet-supported Pt nanocatalysts, Appl. Catal. B Environ. 274 (2020), 118963.

[11] M. Wen, G. Li, H. Liu, J. Chen, T. An, H. Yamashita, Metal-organic framework-based nanomaterials for adsorption and photocatalytic degradation of gaseous pollutants: recent progress and challenges, Environ. Sci. Nano 6 (2019) 1006–1025.

[12] G. Zhan, H.C. Zeng, Hydrogen spillover through Matryoshka-type (ZIFs@)$_{n-1}$ ZIFs nanocubes, Nat. Commun. 9 (2018) 1–12.

[13] Q. Wang, Z. Li, M.A. Bañares, L. Weng, Q. Gu, J. Price, W. Han, K.L. Yeung, A novel approach to high-performance aliovalent-substituted catalysts-2D bimetallic MOF-derived $CeCuO_x$ microsheets, Small 15 (2019), 1903525.

[14] Y. Li, W. Han, R. Wang, L. Weng, A. Serrano-Lotina, M.A. Bañares, Q. Wang, K. L. Yeung, Performance of an aliovalent-substituted $CoCeO_x$ catalyst from bimetallic MOF for VOC oxidation in air, Appl. Catal. B Environ. 275 (2020), 119121.

[15] W. Xu, X. Chen, J. Chen, H. Jia, Bimetal oxide CuO/Co_3O_4 derived from Cu ions partly-substituted framework of ZIF-67 for toluene catalytic oxidation, J. Hazard. Mater. 403 (2021), 123869.

[16] H. Hu, B. Guan, B. Xia, X.W. Lou, Designed formation of Co_3O_4/$NiCo_2O_4$ double-shelled nanocages with enhanced pseudocapacitive and electrocatalytic properties, J. Am. Chem. Soc. 137 (2015) 5590–5595.

[17] G. Zhan, H.C. Zeng, ZIF-67-derived nanoreactors for controlling product selectivity in CO_2 hydrogenation, ACS Catal. 7 (2017) 7509–7519.

[18] M. Wen, S. Song, W. Zhao, Q. Liu, J. Chen, G. Li, T. An, Atomically dispersed Pd sites on Ti-SBA-15 for efficient catalytic combustion of typical gaseous VOCs, Environ. Sci. Nano 8 (2021) 3735–3745.

[19] H. Liu, M. Xu, G. Li, W. Zhang, T. An, Solar-light-triggered regenerative adsorption removal of styrene by silver nanoparticles incorporated in metal–organic frameworks, Environ. Sci. Nano 8 (2021) 543–553.

[20] M. Assebban, A.E. Kasmi, S. Harti, T. Chafik, Intrinsic catalytic properties of extruded clay honeycomb monolith toward complete oxidation of air pollutants, J. Hazard. Mater. 300 (2015) 590–597.

[21] L. Lv, S. Wang, Y. Ding, L. Zhang, Y. Gao, S. Wang, Mechanistic insights into the contribution of Lewis acidity to brominated VOCs combustion over titanium oxide supported Ru catalyst, Chemosphere 263 (2020), 128112.

[22] J.F. Lamonier, T.B. Nguyen, M. Franco, S. Siffert, R. Cousin, Y. Li, X. Yang, B. Su, J. M. Giraudon, Influence of the meso-macroporous ZrO_2-TiO_2 calcination temperature on the pre-reduced Pd/ZrO_2-TiO_2 (1/1) performances in chlorobenzene total oxidation, Catal. Today 164 (2011) 566–570.

[23] M. Piumetti, D. Fino, N. Russo, Mesoporous manganese oxides prepared by solution combustion synthesis as catalysts for the total oxidation of VOCs, Appl. Catal. B Environ. 163 (2015) 277–287.

[24] Y. Liu, H. Dai, J. Deng, S. Xie, H. Yang, W. Tan, W. Han, Y. Jiang, G. Guo, Mesoporous Co_3O_4-supported gold nanocatalysts: highly active for the oxidation of carbon monoxide, benzene, toluene, and o-xylene, J. Catal. 309 (2014) 408–418.

[25] Y. Wang, H. Arandiyan, J. Scott, A. Bagheri, H. Dai, R. Amal, Recent advances in ordered meso/macroporous metal oxides for heterogeneous catalysis: a review, J. Mater. Chem. A 5 (2017) 8825–8846.

[26] Y. Chen, C. Wang, Z. Wu, Y. Xiong, Q. Xu, S.H. Yu, H. Jiang, From bimetallic metal-organic framework to porous carbon: high surface area and multicomponent active dopants for excellent electrocatalysis, Adv. Mater. 27 (2015) 5010–5016.

[27] Y. Zheng, Q. Zhao, C. Shan, S.S. Lu, Yun Su, R. Han, C. Song, N. Ji, D. Ma, Q. Liu, Enhanced acetone oxidation over the CeO_2/Co_3O_4 catalyst derived from metal organic frameworks, ACS Appl. Mater. Interfaces 12 (2020) 28139–28147.

[28] Q. Zhao, Y. Zheng, C. Song, Q. Liu, N. Ji, D. Ma, X. Lu, Novel monolithic catalysts derived from in-situ decoration of Co_3O_4 and hierarchical Co_3O_4@MnO_x on Ni foam for VOC oxidation, Appl. Catal. B Environ. 265 (2020), 118552.

[29] W. Deng, Q. Dai, Y. Lao, B. Shi, X. Wang, Low temperature catalytic combustion of 1, 2-dichlorobenzene over CeO_2-TiO_2 mixed oxide catalysts, Appl. Catal. B Environ. 181 (2016) 848–861.

[30] G. Chen, Y. Zhao, G. Fu, P. Duchesne, L. Gu, Y. Zheng, X. Weng, M. Chen, P. Zhang, C. Pao, Interfacial effects in iron-nickel hydroxide-platinum nanoparticles enhance catalytic oxidation, Science 344 (2014) 495–499.

[31] T. An, J. Liu, G. Li, S. Zhang, H. Zhao, X. Zeng, G. Sheng, J. Fu, Structural and photocatalytic degradation characteristics of hydrothermally treated mesoporous TiO_2, Appl. Catal. A Gen. 350 (2008) 237–243.

[32] J. Liu, T. An, G. Li, N. Bao, G. Sheng, J. Fu, Preparation and characterization of highly active mesoporous TiO_2 photocatalysts by hydrothermal synthesis under weak acid conditions, Microporous Mesoporous Mater. 124 (2009) 197–203.

[33] X. Wang, Y. Liu, T. Zhang, Y. Luo, Z. Lan, K. Zhang, J. Zuo, L. Jiang, R. Wang, Geometrical-site-dependent catalytic activity of ordered mesoporous Co-based spinel for benzene oxidation: in situ DRIFTS study coupled with Raman and XAFS spectroscopy, ACS Catal. 7 (2017) 1626–1636.

[34] U. Menon, V.V. Galvita, G.B. Marin, Reaction network for the total oxidation of toluene over CuO-CeO_2/Al_2O_3, J. Catal. 283 (2011) 1–9.

[35] Y. Guo, Y. Sun, D.-P. Yang, J. Dai, Z. Liu, Y. Chen, J. Huang, Q. Li, Biogenic Pt/$CaCO_3$ nanocomposite as robust catalyst towards benzene oxidation, ACS Appl. Mater. Interfaces 12 (2020) 2469–2480.

[36] W. Tang, X. Wu, D. Li, Z. Wang, G. Liu, H. Liu, Y. Chen, Oxalate route for promoting activity of manganese oxide catalysts in total VOCs' oxidation: effect of calcination temperature and preparation method, J. Mater. Chem. A 2 (2014) 2544.

[37] Z. Wang, J. Liu, Y. Yang, Y. Yu, X. Yan, Z. Zhang, AMn_2O_4 (A = Cu, Ni and Zn) sorbents coupling high adsorption and regeneration performance for elemental mercury removal from syngas, J. Hazard. Mater. 388 (2020), 121738.

[38] W. Song, A.S. Poyraz, Y. Meng, Z. Ren, S. Chen, S.L. Suib, Mesoporous Co_3O_4 with controlled porosity: inverse micelle synthesis and high-performance catalytic CO oxidation at -60°C, Chem. Mater. 26 (2014) 4629–4639.

[39] S. Xie, J. Deng, S. Z, H. Yang, G. Guo, H. Arandiyan, H. Dai, Au-Pd/3DOM Co_3O_4: highly active and stable nanocatalysts for toluene oxidation, J. Catal. 322 (2015) 38–48.

[40] X. Weng, P. Sun, Y. Long, Q. Meng, Z. Wu, Catalytic oxidation of chlorobenzene over $Mn_xCe_{1-x}O_2$/HZSM-5 catalysts: a study with practical implications, Environ. Sci. Technol. 51 (2017) 8057–8066.

[41] F. Hao, Y. Gao, J. Liu, R. Dudek, L. Neal, S. Wang, P. Liu, F. Li, Zeolite-assisted core-shell redox catalysts for efficient light olefin production via cyclohexane redox oxidative cracking, Chem. Eng. J. 409 (2021), 128192.

[42] H. Xiao, J. Zhang, X. Wang, Q. Zhang, H. Xie, Y. Han, Y. Tan, A highly efficient Ga/ZSM-5 catalyst prepared by formic acid impregnation and in situ treatment for propane aromatization, Catal. Sci. Technol. 5 (2015) 4081–4090.

[43] P. Sun, W. Wang, X. Dai, X. Weng, Z. Wu, Mechanism study on catalytic oxidation of chlorobenzene over $Mn_xCe_{1-x}O_2$/H-ZSM5 catalysts under dry and humid conditions, Appl. Catal. B Environ. 198 (2016) 389–397.

[44] V.B. Kazansky, M.V. Frash, R.A.V. Santen, A quantum-chemical study of adsorbed nonclassical carbonium ions as active intermediates in catalytic transformations of paraffins. II. Protolytic dehydrogenation and hydrogen-deuterium hetero-isotope exchange of paraffins on high-silica zeolites, Catal. Lett. 28 (1994) 211–222.

[45] Z. Hou, L. Dai, Y. Liu, J. Deng, H.J. Dai, Highly efficient and enhanced sulfur resistance supported bimetallic single-atom palladium-cobalt catalysts for benzene oxidation, Appl. Catal. B Environ. 285 (2020), 119844.

[46] K. Vikrant, K.H. Kim, V. Kumar, D.A. Giannakoudakis, D.W. Boukhvalov, Adsorptive removal of an eight-component volatile organic compound mixture by Cu-, Co-, and Zr-metal-organic frameworks: experimental and theoretical studies, Chem. Eng. J. 397 (2020), 125391.

[47] Y. Zheng, Y. Su, C. Pang, L. Yang, C. Song, N. Ji, D. Ma, X. Lu, R. Han, Q. Liu, Interface-enhanced oxygen vacancies of $CoCuO_x$ catalysts in situ grown on monolithic Cu foam for VOC catalytic oxidation, Environ. Sci. Technol. (2021).

[48] X. Chen, X. Chen, S. Cai, J. Chen, W. Xu, H. Jia, J. Chen, Catalytic combustion of toluene over mesoporous Cr_2O_3-supported platinum catalysts prepared by in situ pyrolysis of MOFs, Chem. Eng. J. 334 (2018) 768–779.

[49] W. Jiang, Y. Feng, Y. Zeng, Y. Yao, L. Gu, H. Sun, W. Ji, H. Arandiyan, C.T. Au, Establishing high-performance Au/cobalt oxide interfaces for low-temperature benzene combustion, J. Catal. 375 (2019) 171–182.

[50] J. Chen, X. Chen, X. Chen, W. Xu, Z. Xu, H. Jia, J. Chen, Homogeneous introduction of CeO_y into MnO_x-based catalyst for oxidation of aromatic VOCs, Appl. Catal. B Environ. 224 (2017) 825–835.